Desalination and Water Treatment
www.deswater.com

doi: 10.1080/19443994.2013.871339

53 (2015) 2712–2719
March

Taylor & Francis
Taylor & Francis Group

Environmental remediation from aqueous mercury (II) by photocatalytic reduction using a coupled SnO_2–Co_3O_4 nanocomposite

R.M. Mohamed[a,b,c,*], H.A. Gazzaz[a]

[a]*Department of Chemistry, Faculty of Science, King Abdulaziz University, P. O. Box 80203, Jeddah 21589, Saudi Arabia Tel. +0099540715648; Fax: +00966540715648; email: redama123@yahoo.com*
[b]*Advanced Materials Department, Central Metallurgical R & D Institute, P.O. Box 87 Helwan, Cairo 11421, Egypt*
[c]*Center of Excellence in Environmental Studies, King Abdulaziz University, P.O. Box 80216, Jeddah 21589, Saudi Arabia*

Received 15 May 2013; Accepted 17 November 2013

ABSTRACT

Coupled SnO_2–Co_3O_4 nanocomposite has been prepared by a simple co-precipitation method. The prepared coupled composites were tested for photocatalytic reduction of Hg^{2+} under visible light. The characterization of catalyst properties was done by the means of X-ray diffraction, Brunauer–Emmett–Teller, transmission electron microscopy, and ultraviolet–vis spectra. The presence of Co_3O_4 in a SnO_2 composite can change the surface properties to achieve sensitivity to visible light. A coupled SnO_2–Co_3O_4 nanocomposite can eliminate the recombination of electron-hole pairs in the catalyst. The results demonstrated that the optimum mol% of SnO_2:Co_3O_4 was 1:3, as this resulted in the greatest performance of the photocatalyst and a reduction of about 100% of Hg^{2+} in a 100 ppm solution in just 30 min. Additionally, the quantum yield for Hg formation by 1Sn:3Co sample is higher than that of Co and Sn samples by about one and six times, respectively.

Keywords: A coupled SnO_2–Co_3O_4; Nanocomposite; Visible photocatalyst; Mercury

---

1. Introduction

Mercury has some applications in various industries; and at present, its use is mostly forbidden due to its higher level of toxicity. Mercury(II) is also a frequent component of industrial wastewater and is used in agricultural products such as pesticides, fungicides, herbicides, insecticides, and bactericides, which are currently forbidden. Mercury is also used in other industries such as chlorine-alkali, paints, pharmaceuticals, electronics, and cosmetics, among others [1,2]. In aquatic systems, mercury is often converted by bacteria into methyl mercury, and hence magnified hundred to thousand times as it moves through the aquatic food chain, posing potential risks to both humans and wildlife that consume fish [3]. Heterogeneous photocatalysis is a convenient tool for mercury reduction because it uses inexpensive chemicals [4–6].

The wide varieties of electronic and chemical properties of metal oxides make them exciting materials for both basic research and technological applications. Metal oxides span a wide range of electrical and optical properties from wide-band gap insulators and lasers to metallic, superconducting, and field-emitting materials. Enormous efforts are being directed towards the development of nanometer-sized metal oxides in studies related to their fundamental mecha-

---

*Corresponding author.

1944-3994/1944-3986 © 2013 Balaban Desalination Publications. All rights reserved.

nisms such as size and/or quantum effects and towards the application of these materials [7].

Semiconductors with wide band gaps show greater stability than those with small and medium band gaps, but have lower light-harvesting ability in visible light and as such. Attempts towards coupling semiconductors with different band gaps are considered to be a good approach to prepare photocatalysts possessing both high activity and good stability. In coupled semiconductors, the excited electrons can transfer from the high-conduction band to a lower one, hence leading to an efficient separation of photogenerated electron-hole pairs [7].

Photocatalytic activity enhancements over coupled semiconductors, including CdS/TiO_2 [8], ZnS/TiO_2 [9], Cu_2O/TiO_2 [10], CuO/TiO_2 [11,12], WO_3/TiO_2 [13], $BaTiO_3$/TiO_2 [14], SnO_2/TiO_2 [15], Ta_2O_5/TiO_2 [16], and CuO/Al_2O_3/TiO_2 [17], have been investigated extensively. While SnO_2 shows good activity and stability under irradiation in both acidic and basic media, pure SnO_2 has much lower photocatalytic activity even under UV irradiation due to its large band gap (3.8 eV) [18]. The CuO/SnO_2 nanocomposites have been studied as gas sensor materials [19–21] as well as electrochemical materials [22]. In order to improve the photocatalytic activity of SnO_2, coupling of SnO_2 must be carried out with another semiconductor with a lower band gap.

The Co_3O_4 is a p-type semiconductor with a small band gap. If the SnO_2 is coupled with the Co_3O_4, n-SnO_2/p-Co_3O_4 heterojunctions can be formed in the interface. The photogenerated electrons from SnO_2 can easily migrate to Co_3O_4. This favors the separation of photogenerated electrons with holes, leading to an enhancement of photocatalytic activity. Regarding the photocatalytic reduction of Hg^{2+} using a coupled SnO_2–Co_3O_4 nanocomposite, less information is available, which gives us the chance to make preparations for and to investigate the photocatalytic performance of SnO_2–Co_3O_4 nanocomposite. SnO_2–Co_3O_4 photocatalysts have been prepared by simple co-precipitation method and are characterized by XRD, ultraviolet–vis spectra (UV–vis), transmission electron microscopy (TEM), and Brunauer–Emmett–Teller (BET). Effects of different variables on the photocatalytic reduction of Hg^{2+} have been investigated in detail, including Co_3O_4 content, photocatalyst loading, and reaction time.

2. Materials and experimental procedures

2.1. Materials

All chemicals used throughout the present study were of the A.R. grade and were purchased from Sigma. $SnCl_4 \cdot 5H_2O$ was used as the source of Sn; $CoCl_2 \cdot 6H_2O$ as the source of Co; and NaOH was used to adjust the pH balance.

2.2. SnO_2 nanoparticle synthesis

The co-precipitation method was carried out in order to prepare SnO_2 nanoparticles using $SnCl_4 \cdot 5H_2O$ as a starting material. As is typical, $SnCl_4$ at a desired molar ratio was dissolved in distilled water. After continuously stirring at 80°C, the NaOH solution was added as a precipitating agent until a pH of 11 was reached. The precipitate was dried overnight at 100°C and calcined at 550°C for 5 h to obtain SnO_2 nanoparticles (Sn).

2.3. Co_3O_4 nanoparticles synthesis

The Co_3O_4 nanoparticles were prepared by the co-precipitation route in which $CoCl_2 \cdot 6H_2O$ was dissolved in distilled water with an aqueous solution of NaOH while stirring at 80°C until complete precipitation was achieved at a pH value of almost 11. Next, the precipitate was filtered and then washed thoroughly with distilled water until it was free of Cl ions. It was then finally dried at 100°C overnight and calcined at 550°C for 5 h to obtain Co_3O_4 nanoparticles (Co).

2.4. SnO_2–Co_3O_4 nanocomposites synthesis

In the co-precipitation method, an adequate amount of $SnCl_4 \cdot 5H_2O$ and $CoCl_2$ with appropriate molar ratios (3:1; 2:1; 1:1; 1:2, and 1:3) were dissolved in distilled water. The obtained mixtures were continuously stirred at 80°C, followed by adding the NaOH solution which is considered to be a precipitating agent. After that, filtration and washing were carried out, followed by calcination at 550°C for 5 h to obtain SnO_2–Co_3O_4 nanocomposites. The obtained samples with different molar ratios of Sn:Co (3:1; 2:1; 1:1; 1:2, and 1:3) were labeled as 3Sn–1Co; 2Sn–1Co; 1Sn–1Co; 1Sn–2Co; and 1Sn–3Co, respectively.

2.5. Characterization

X-ray diffraction (XRD) analysis was carried out at room temperature by means of a Bruker axis D8 using Cu Kα radiation (λ = 1.540 Å). Specific surface area was calculated from measurements of N_2 adsorption using a Nova 2000 series Chromatech apparatus at 77 K. Prior to the measurements, all samples were treated under vacuum at 250°C for 2 h. The band gaps of the samples were identified by UV–vis diffuse reflectance spectra (UV–vis-DRS) in air at room temperature in the wavelength range of 200–800 nm using a UV/vis/NIR spectrophotometer (V-570, JASCO, Japan). TEM was recorded with a JEOL-JEM-1230 microscope and prepared samples were suspended in ethanol. This was followed by ultrasonication for 30 min, after which a small amount of this solution was transferred onto a carbon-coated copper grid and dried before loading the sample into the TEM.

2.6. Photocatalytic activity tests

The photocatalytic reduction of Hg(II) was conducted in a glass reactor. Visible light was provided by way of a 300 W Xe lamp with a 400 nm cut-off filter to ensure the desired irradiation. In a typical run, a weight of the catalyst was stirred into 500 mL of aqueous Hg(II) solution (100 ppm) and the solution's pH was adjusted to 4.0 using formic acid. Prior to photoreaction, air was pumped into the reaction in the dark for a duration of 30 min to achieve the adsorption–desorption equilibrium. The light source was then turned on and the solution was continuously stirred throughout the irradiation to maintain catalyst suspension. The temperature of the suspension was maintained at 25˚C by circulating water through an external cooling jacket and exposing the system to air. At regular intervals, samples of the suspension were withdrawn and filtered through a 0.45-μm Millipore filter. The concentration of mercury(II) in solution was determined using a UV/vis/NIR spectrophotometer (V-570, JASCO, Japan), which was used for all spectrophotometric measurements (wavelength 253.7).

The photocatalytic reduction efficiency of Hg^{2+} was estimated by applying the following equation:

$$\%\,\text{Photocatalytic reduction of}\,\text{Hg}^{2+} = (C_0 - C)/C_0 \times 100 \tag{1}$$

where "C_0" is the initial concentration of Hg^{2+} and "C" is the residual Hg^{2+} concentration in solution.

The photonic efficiency was calculated for each experiment as the ratio of the Hg formation rate and the incident light intensity as given in the following equation:

$$\xi = \frac{r \times 100}{I} \tag{2}$$

where "ξ" is the photonic efficiency (%), "*r*" is the photoreduction of Hg^{2+}, and "*I*" is the incident photon flux (3.37×10^{-6} Ein $L^{-1}s^{-1}$). The quantum yield of Hg formation could be determined as $\Phi = \xi/\text{Fs}$, where "ξ" is photonic efficiency and "Fs" is the fraction of light observed by tested catalyst.

3. Results and discussion

3.1. Characterization

3.1.1. XRD analysis

X-ray powder diffraction (XRD) was used to follow the phase changes undergone by the materials by monitoring the d-lines corresponding to the interlayer distance of the material and its harmonics. Fig. 1 represents the XRD diffractograms of the Sn, Co, and SnO_2–Co_3O_4 nanocomposites. The following section describes what was reveled upon inspection of the obtained XRD diffractograms as given in Fig. 1.

Based on the JCPDS card No. 88-0287, the SnO_2 *d*-lines could be detected. In addition, according to JCPDS card No. 78-1970, Co_3O_4 diffraction lines could be detected. SnO_2 phase exists as a major phase at molar ratios of 2:1 and 3:1 (Sn:Co). Furthermore, by increasing the content of Co at molar ratios of 1:2 and 1:3 (Sn:Co), the coexistence of Co_3O_4 and SnO_2 phases increases, the peak intensity of Co_3O_4 phase becomes more pronounced, and the sharpness of diffraction lines increases while those pertaining to SnO_2 become broader.

3.1.2. BET analysis

Textural properties were studied by nitrogen adsorption for Sn, Co, and SnO_2–Co_3O_4. The main data obtained from the BET analysis are summarized in Table 1. Assessment of the obtained data revealed

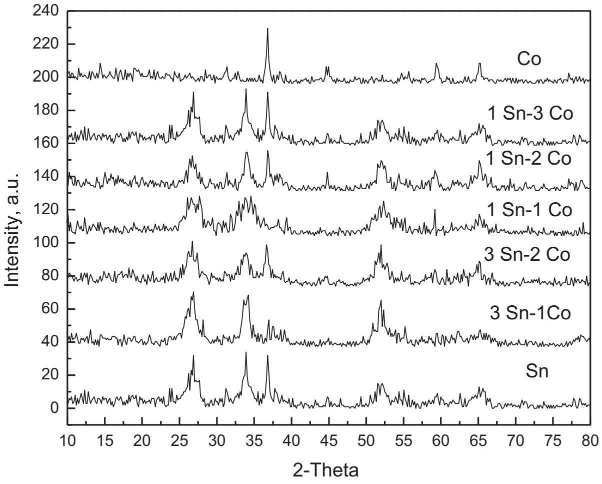

Fig. 1. XRD patterns of SnO_2, Co_3O_4, and SnO_2–Co_3O_4 nanocomposites.

that the values of S_{BET} increase with the increase of % Co content. Furthermore, the lower value obtained for the oxide with low Co content is in agreement with the narrow peaks observed in the XRD diagram with such oxide.

3.1.3. Optical properties

The optical absorbance UV–vis diffuse reflectance spectra of SnO_2, Co_3O_4, and SnO_2–Co_3O_4 nanocomposites is displayed in Fig. 2. Increasing the content of Co_3O_4 led to a parallel increase in the absorption (visible region), suggesting that it is possible to use SnO_2–Co_3O_4 nanocomposites as photocatalysts under visible light irradiation.

Table 2 compiled the calculated band gap (E_g) depending on the corresponding absorption edges. It can be seen from the compiled data, as displayed in Table 2, that the calcinations of SnO_2–Co_3O_4 nanocomposites at 550°C for 5 h had led to the appearance of a mixture of Co_3O_4 and SnO_2 phases, which in turn led to the overlapping of the corresponding components in the coupled oxides. In addition, it can also be seen that the band gap energy changed with the change in Co_3O_4 content, indicating an inverse correlation between Co_3O_4 content and the band gap energy of the coupled SnO_2–Co_3O_4 photocatalyst.

3.1.4. TEM

TEM yields information about the internal structure of materials. The TEM images of SnO_2, Co_3O_4, and SnO_2–Co_3O_4 nanocomposites are shown in Fig. 3. The following section describes what could be observed followed by a careful examination of the obtained results.

The values of nanoparticle size pertaining to SnO_2 and SnO_2–Co_3O_4 consisted of about 20–33 nm, whereas Co_3O_4 nanoparticles are much smaller (about 6–10 nm). The highest size for SnO_2–Co_3O_4 nanocomposites could be attributed to larger SnO_2 and smaller Co_3O_4 nanoparticles. Nevertheless, many values of small-sized Co_3O_4 nanoparticles became more observable. No SnO_2 nanoparticles were observed in the TEM images for the ratios from 3Sn–1Co to 1Sn–3Co.

Table 1
BET surface of SnO_2, Co_3O_4, and SnO_2–Co_3O_4 nanocomposites

Catalyst systems	S_{BET} (m^2/g)
Sn	30
3Sn–1Co	34
2Sn–1Co	38
1Sn–1Co	41
1Sn–2Co	43
1Sn–3Co	47
Co	52

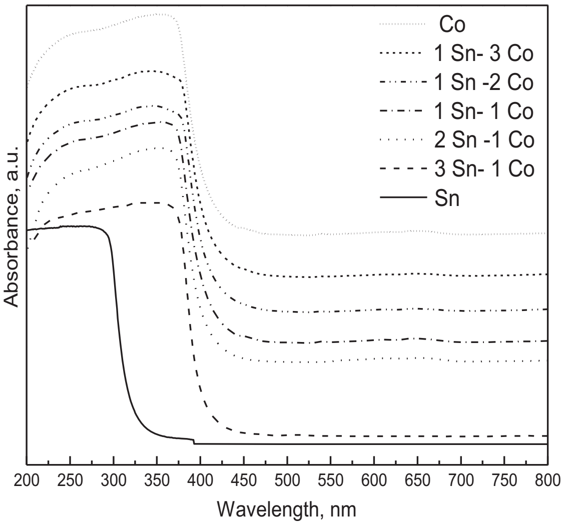

Fig. 2. UV–vis absorption spectra of SnO_2, Co_3O_4, and SnO_2–Co_3O_4 nanocomposites.

Table 2
Band gap and quantum yield of SnO_2, Co_3O_4, and SnO_2–Co_3O_4 nanocomposites

Catalyst systems	Band gap, eV	Quantum yield, Φ
Sn	3.7	0.0149
3Sn–1Co	2.9	0.0467
2Sn–1Co	2.7	0.0673
1Sn–1Co	2.5	0.0766
1Sn–2Co	2.4	0.0841
1Sn–3Co	2.3	0.0935
Co	2.2	0.0804

3.2. Test for photocatalytic activity towards Hg^{2+} reduction

Within the frame of the present study, Hg^{2+} reduction was taken as a model test reaction to study the photocatalytic activity of the system under consideration.

3.2.1. Study on the effect of Co and Sn content

Fig. 4 shows the photocatalytic reduction of Hg^{2+} pertaining to Sn, Co, and Sn–Co nanocomposites under visible light. The reaction was conducted under the following conditions: 100 ppm Hg^{2+} concentration;

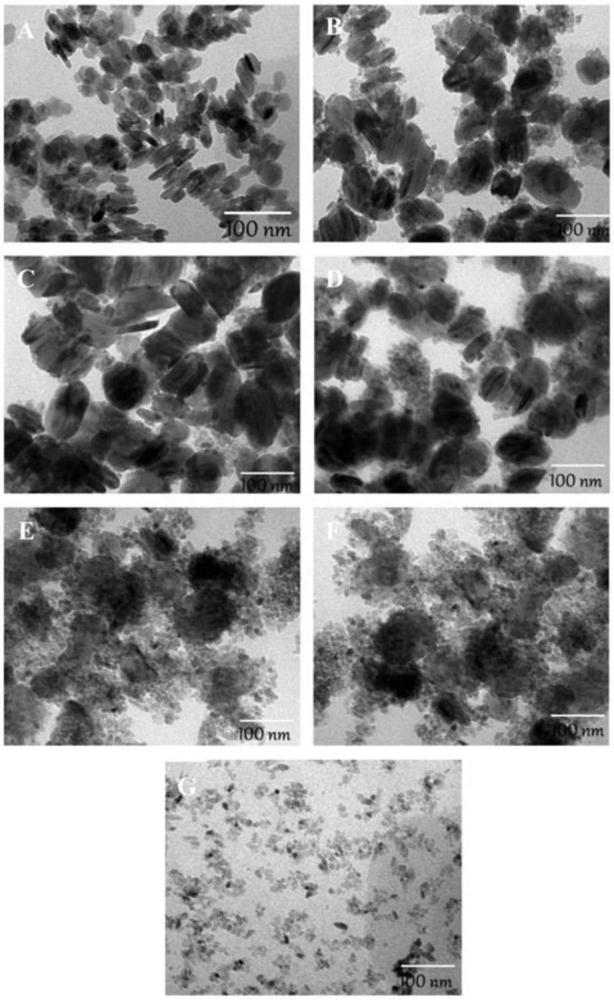

Fig. 3. TEM images of SnO_2, Co_3O_4, and SnO_2–Co_3O_4 nanocomposites, whereas (A) Sn; (B) 3Sn–1Co; (C) 2Sn–1Co; (D) 1Sn–1Co; (E) 1Sn–2Co; (F) 1Sn:3Co; and (G) Co.

500 ml volume of Hg^{2+} solution, and 0.4 g weight of catalyst.

It is clear from the obtained data of the investigated catalytic systems that in the Sn sample, no reduction of Hg^{2+} occurred when subjected to visible light (k > 420 nm) irradiation for 60 min. On the contrary, the presence of Co and Sn–Co suggests that there is an observed increase in Hg^{2+} reduction that is parallel to the rise in irradiation time (t). In the light of these results, the photocatalytic activity increased in the following order: Sn < 3Sn–1Co < 2Sn–1Co < 1Sn–1Co < Co < 1Sn–2CO < 1Sn–3Co.

This is most likely a result of the combined action of many factors such as composition, specific surface area, adsorption capacity for Hg^{2+}, band gap, and microstructure. It is supposed that the composition of SnO_2–Co_3O_4 sample nanocomposites should play a predominant role in their photocatalytic activity.

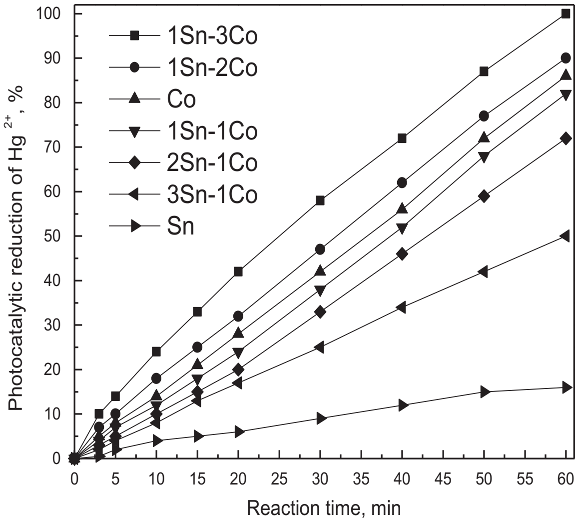

Fig. 4. Photocatalytic reduction of Hg^{2+} by SnO_2, Co_3O_4, and SnO_2–Co_3O_4 nanocomposites.

On the basis of the observed decreasing values of activity with the decrease of Co content in 3Sn–1Co system, a small fraction of SnO_2 is not likely to make contact with Co_3O_4 (i.e. the surfaces of a portion of SnO_2 nanoparticles were either bare or insufficiently covered with Co_3O_4 nanoparticles), which restricted the efficient interfacial electron transfer from Co_3O_4 to SnO_2. As a result, their photocatalytic activities cannot be enhanced to the greatest extent. On the other hand, the much greater the Co content in the Sn–Co nanocomposites, the maximum their photocatalytic activities. This was mainly due to the ability of Co_3O_4 to be more active than SnO_2 under visible light (k > 420 nm) irradiation. Furthermore, the high Sn content in the Sn–Co surface possibly obscured the light irradiation on Co_3O_4 and hampered the contact of SnO_2 with aqueous Hg^{2+}. Consequently, there must be an optimum composition for a SnO_2–Co_3O_4 nanocomposite to achieve the highest photocatalytic activity. 1Sn–3Co is considered to be a suitable content of Co_3O_4 (75 mass%) and possessed the highest photocatalytic activity among the SnO_2–Co_3O_4 nanocomposites.

3.2.2. Effect of photocatalyst concentration on photocatalytic reduction of Hg^{2+}

The relative concentration of the photocatalyst is another important parameter of photocatalytic reduction of Hg^{2+} under visible light irradiation. Concentrations of the 1Sn–3Co sample ranging from

0.2 to 1.6 g L^{-1} in 100 ppm Hg^{2+} solutions were employed in this study. As shown in Fig. 5, an increase in the photocatalytic reduction of Hg^{2+} efficiency was observed with the increase in catalyst concentration from 0.2 to 1.2 g L^{-1}. Beyond the concentration level of 1.2 g L^{-1}, however, further increase in the photocatalyst concentration was seen to be less effective in the photocatalytic reduction of Hg^{2+}. As such, it can be seen that the increase in the photocatalyst concentration increased the number of active sites on the photocatalyst [23] and consequently, the number of Hg^{2+} and photons absorbed increased. However, as the photocatalyst concentration level increased to above 1.2 g L^{-1}, the rate constants decreased due to the blocking of light penetration by the excessive concentration of photocatalysts [24].

3.2.3. Photocatalyst recycling process

The aim of the catalyst recycling process is to evaluate the practical application of photocatalysts in order to develop a heterogeneous photocatalysis technology for wastewater treatment and accordingly, the photocatalytic activity of the recycled 1Sn–3Co sample catalyst was carried out. Examination of the obtained data revealed that the photocatalytic reduction of Hg^{2+} efficiency was 99% during the first five cycles as shown in Fig. 6 and during that time, the separation of the photocatalyst was found to be effective; hence, suggesting that the photocatalyst is basically stable and offers promising possibilities for environmental remediation.

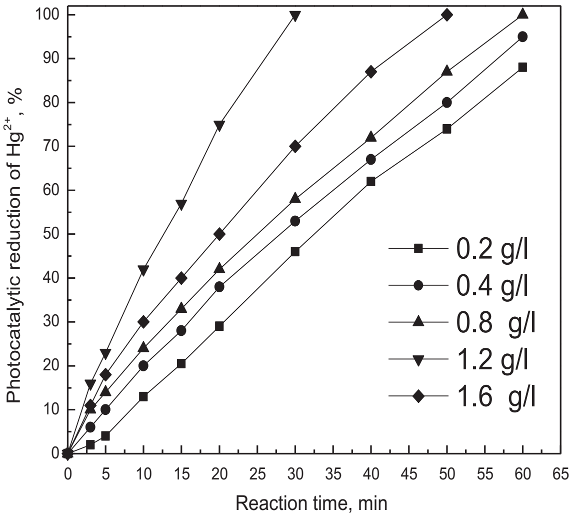

Fig. 5. Effect of photocatalyst amount on photocatalytic reduction of Hg^{2+}.

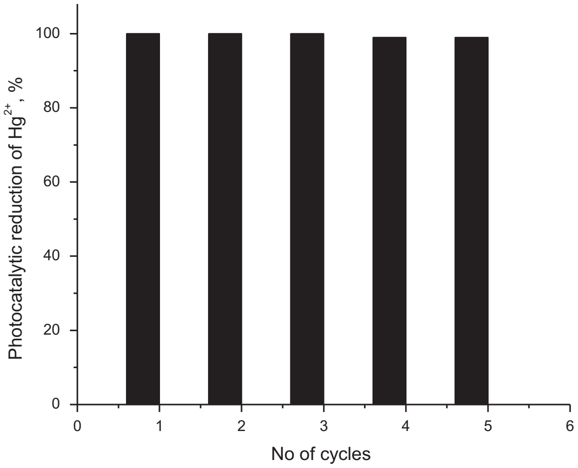

Fig. 6. Recycle and reuse of photocatalysts for photocatalytic reduction of Hg^{2+}.

3.2.4. Photocatalytic mechanism

Considering the irradiation of semiconductor photocatalysts using light together with photon energies greater than or equal to their band gaps, an excitation of the electrons exists in their valence bands to their conduction bands, consequently leaving behind an equal amount of electron holes in their main valence bands. Next, a portion of the photogenerated electrons (e^-) and holes (h^+) might be expelled from the surface of the photocatalyst, after which they become involved in the redox reactions together with the adsorbed species.

In light of the process including SnO_2–Co_3O_4 nanocomposites used for photocatalytic reduction of aqueous Hg(II), one could observe that no more reducing agents or hole scavengers were added. For that, it was proposed that the photogenerated electrons were reduced from Hg(II) to Hg, while the holes responsible for the oxidation of water were reduced to O_2.

The proposed mechanism is shown in the following equations:

$$\mathrm{SnO_2 - Co_3O_4} + h\gamma \rightarrow \mathrm{SnO_2 - Co_3O_4}(e^- + h^+) \qquad (3)(3)$$

$$\mathrm{Hg(II)} + 2e \rightarrow \mathrm{Hg} \qquad (4)(4)$$

$$\mathrm{2H_2O + 4h \rightarrow O_2 + 4H^+} \qquad (5)(5)$$

Fig. 7 displays the relation between the separation of the efficient charge and the lifetime of the charge carriers. For SnO_2–Co_3O_4 nanocomposites under visible light irradiation, the electron in the valence

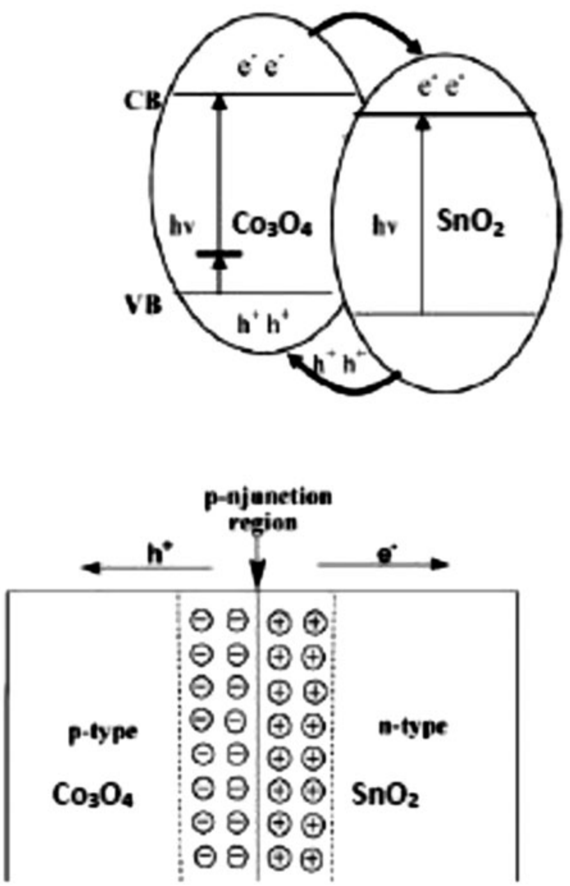

Fig. 7. *p–n* Junction formation model and the schematic diagram of the electron-hole separation process.

band of Co_3O_4 can be excited to its conduction band with continuous generation of an equal amount of holes in its valence band, whereas SnO_2 has low response ability because of its wide band gap value (E_g = 3.7 eV), and a lower negativity of valence band pertaining to SnO_2 than that of Co_3O_4. Therefore, the migration of photogenerated electrons from the Co_3O_4 conduction band to that of SnO_2 could be easier. Thus, photogenerated electrons and holes in Co_3O_4 can be effectively separated, and so their recombination will be decreased.

4. Conclusions

SnO_2–Co_3O_4 nanocomposite photocatalyst was successfully prepared with the co-precipitation method. This method is simple and cost-effective, and is thus suitable for large-scale production of SnO_2–Co_3O_4 nanocomposite. The prepared composites were analyzed by XRD, TEM, UV–vis, and BET. Through photocatalytic experiments using aqueous Hg(II) as a target contaminant under visible light ($k > 420$ nm) irradiation, the following results were obtained: (1) the photocatalytic activities of SnO_2–Co_3O_4 nanocomposites depended on their composition, and 1Sn–3Co with a suitable content (75 mass%) of Co_3O_4 possessed the highest photocatalytic activity among SnO_2–Co_3O_4 nanocomposites; (2) the 1Sn–3Co sample also exhibited higher photocatalytic efficiencies than SnO_2 and Co_3O_4; and (3) the 1Sn–3Co sample demonstrated a certain degree of photocatalytic stability. Optimization of reaction conditions leads to a conclusion that a SnO_2–Co_3O_4 and a use of 0.6 g of the catalyst on a 500-mL, 100-ppm Hg^{2+} solution yield 100% reduction of Hg^{2+} within 30 min irradiation under visible light. The high, visible, and light-driven photocatalytic activity as well as the good stability of the SnO_2-Co_3O_4 nanocomposite enables it to be a promising photocatalyst in the efficient utilization of solar energy for the treatment of Hg(II) wastewater.

References

[1] E.M. Fournière, A.G. Leyva, E.A. Gautier, M.I. Litter, Treatment of phenyl mercury salts by heterogeneous photocatalysis over TiO_2, Chemosphere 69 (2007) 682–688.

[2] J.B. Zambrano, S. Laborie, P. Viers, M. Rakib, G. Durand, Mercury removal from aqueous solutions by complexation—ultrafiltration, Desalination 144 (2002) 201–206.

[3] N. Serpone, Y.K. Ah-You, T.P. Tran, R. Harris, E. Pelizzetti, H. Hidaka, AM1 simulated sunlight photoreduction and elimination of Hg(II) and CH_3Hg(II) chloride salts from aqueous suspensions of titanium dioxide, Sol. Energy 39 (1987) 491–498.

[4] N. Serpone, E. Borgarello, E. Pelizzetti, Photoreduction and photodegradation of inorganic pollutants: II. Selective reduction and recovery of Au, Pt, Pd, Rh, Hg, and Pb, in: M. Schiavello (Ed.), Photocatalysis and Environment, Kluwer Academic, Dordrecht, 1988, p. 527.

[5] G.G. Lenzi, B.V.C. Fávero, S.M.L. Colpini, H. Bernabe, L.M. Baesso, S. Specchia, A.A.O. Santos, Photocatalytic reduction of Hg(II) on TiO_2 and Ag/TiO_2 prepared by the sol-gel and impregnation methods, Desalination 270(1–3) (2011) 241–247.

[6] J.M. López-Muñoz, J. Aguado, A. Arencibia, R. Pascual, Mercury removal from aqueous solutions of $HgCl_2$ by heterogeneous photocatalysis withTiO_2, Appl. Catal., A 104(3–4) (2011) 20–228.

[7] R.M. Mohamed, D.L. McKinney, W.M. Sigmund, Enhanced nanocatalysts, Mater. Sci. Eng., R 73 (2012) 1–13.

[8] T. Xu, F. Zou, Y. Yu, J. Zhi, Synthesis and characterization of CdSexTe1−x sensitized TiO_2 solar cell with enhanced photovoltaic properties, Mater. Lett. 96 (2013) 8–11.

[9] D.X. Yu, Y.Q. Wu, C.S. Jiang, H.Y. Guo, Nanoscale ZnS/TiO_2 composites: Preparation, characterization, and visible-light photocatalytic activity, Mater. Char. 57 (2006) 333–341.

[10] L. Likun, X. Leilei, S. Weidong, G. Jianguo, Facile preparation and size-dependent photocatalytic activity of Cu_2O nanocrystals modified titania for hydrogen evolution, Int. J. Hydrogen Energy 38 (2013) 816–822.

[11] A.J. Simamora, T.L. Hsiung, F.C. Chang, T.C. Yang, C.Y. Liao, H. Paul Wang, Photocatalytic splitting of seawater and degradation of methylene blue on CuO/nano TiO_2, Int. J. Hydrogen Energy 37 (2012) 13855–13858.

[12] P.S. Xu, D.D. Sun, Significant improvement of photocatalytic hydrogen generation rate over TiO_2 with deposited CuO, Int. J. Hydrogen Energy 34 (2009) 6096–6104.

[13] J. Yang, X. Zhang, H. Liu, C. Wang, S. Liu, P. Sun, L. Wang, Y. Liu, Heterostructured TiO_2/WO_3 porous microspheres: Preparation, characterization and photocatalytic properties, Catal. Today 201 (2013) 195–202.

[14] R. Li, Q. Li, L. Zong, X. Wang, J. Yang, $BaTiO_3/TiO_2$ heterostructure nanotube arrays for improved photoelectrochemical and photocatalytic activity, Electrochim. Acta 91 (2013) 30–35.

[15] R. Sasikala, A. Shirole, V. Sudarsan, T. Sakuntala, C. Sudakar, R. Naik, Highly dispersed phase of SnO_2 on TiO_2 nanoparticles synthesized by polyol-mediated route: Photocatalytic activity for hydrogen generation, Int. J. Hydrogen Energy 34 (2009) 3621–3630.

[16] M. Stodolny, M. Laniecki, Synthesis and characterization of mesoporous Ta_2O_5/TiO_2 photocatalysts for water splitting, Catal Today 142 (2009) 314–319.

[17] T. Miwa, S. Kaneco, H. Katsumata, T. Suzuki, K. Ohta, C.S. Verma, Photocatalytic hydrogen production from aqueous methanol solution with $CuO/Al_2O_3/TiO_2$ nanocomposite, Int. J. Hydrogen Energy 35 (2010) 6554–6560.

[18] W. Zhou, M. Tan, Synthesis and optical properties of SnO_2–CuO nanocomposite, Optik—Int. J. Light Electron Opt. 123 (2012) 2171–2173.

[19] H.Z. Zhou, X.Q. Cao, H. Huang, P. Yang, Y. Hu, Study on sensing mechanism of CuO/SnO_2 gas sensors, Mater. Sci. Eng. B 99 (2003) 44–47.

[20] T. Pagnier, M. Boulova, A. Galerie, A. Gaskov, G. Lucazeau, Reactivity of SnO_2/CuO nanocrystalline materials with H_2S: A coupled electrical and Raman spectroscopic study, Sens. Actuator, B Chem. 71 (2000) 134–139.

[21] S.I. Hwang, K.J. Choi, J.S. Kim, Y.K. Dong, H.J. Kwon, K.B. Ju, Enhanced H_2S sensing characteristics of SnO_2 nanowires functionalized with CuO, Sensor Actuat. B Chem. 142 (2009) 105–110.

[22] C. Li, W. Wei, M.S. Fang, X.H. Wang, Y. Zhang, H.Y. Gui, A novel CuO-nanotube/SnO_2 composite as the anode material for lithium ion batteries, J. Power Sources 195 (2010) 2939–2944.

[23] J. Nishio, M. Tokumura, H.T. Znad, Y. Kawase, Photocatalytic decolorization of azo-dye with zinc oxide powder in an external UV light irradiation slurry photoreactor, J. Hazard. Mater. 138 (2006) 106–115.

[24] M. Saquib, M.A. Tariq, M.M. Haque, M. Muneer, Photocatalytic degradation of disperse blue 1 using UV/TiO_2/H_2O_2 process, J. Environ. Manage. 88 (2008) 300–306.